

Article

Expanding the Range: AuCu Metal Aerogels from H₂O and EtOH

Maximilian Georgi ¹, Johannes Kresse ¹, Karl Hiekel ¹, René Hübner ²  and Alexander Eychmüller ^{1,*}

¹ Physical Chemistry, TU Dresden, 01069 Dresden, Germany; maximilian.georgi@tu-dresden.de (M.G.); johannes.kresse@tu-dresden.de (J.K.); karl.hiekel@tu-dresden.de (K.H.)

² Institute of Ion Beam Physics and Materials Research, Helmholtz-Zentrum Dresden-Rossendorf e.V., 01328 Dresden, Germany; r.huebner@hzdr.de

* Correspondence: alexander.eychmueller@tu-dresden.de

Abstract: Due to their self-supporting and nanoparticulate structure, metal aerogels have emerged as excellent electrocatalysts, especially in the light of the shift to renewable energy cycles. While a large number of synthesis parameters have already been studied in depth, only superficial attention has been paid to the solvent. In order to investigate the influence of this parameter with respect to the gelation time, crystallinity, morphology, or porosity of metal gels, Au_xCu_y aerogels were prepared in water and ethanol. It was shown that although gelation in water leads to highly porous gels (60 m²g⁻¹), a CuO phase forms during this process. The undesired oxide could be selectively removed using a post-washing step with formic acid. In contrast, the solvent change to EtOH led to a halving of the gelation time and the suppression of Cu oxidation. Thus, pure Cu aerogels were synthesized in addition to various bimetallic Au₃X (X = Ni, Fe, Co) gels. The faster gelation, caused by the lower permittivity of EtOH, led to the formation of thicker gel strands, which resulted in a lower porosity of the Au_xCu_y aerogels. The advantage given by the solvent choice simplifies the preparation of metal aerogels and provides deeper knowledge about their gelation.



Citation: Georgi, M.; Kresse, J.; Hiekel, K.; Hübner, R.; Eychmüller, A. Expanding the Range: AuCu Metal Aerogels from H₂O and EtOH. *Catalysts* **2022**, *12*, 441. <https://doi.org/10.3390/catal12040441>

Academic Editor: Leonarda Francesca Liotta

Received: 24 March 2022

Accepted: 12 April 2022

Published: 14 April 2022

Publisher's Note: MDPI stays neutral with regard to jurisdictional claims in published maps and institutional affiliations.



Copyright: © 2022 by the authors. Licensee MDPI, Basel, Switzerland. This article is an open access article distributed under the terms and conditions of the Creative Commons Attribution (CC BY) license (<https://creativecommons.org/licenses/by/4.0/>).

Keywords: metal; aerogel; gold; copper; ethanol; water; solvent; bimetallic; porous; one-step

1. Introduction

Metal aerogels have a high potential for application as electrocatalysts, e.g., in the field of fuel cell technology or the sustainable closure of the carbon cycle [1–10]. This is primarily a result of their unusual, advantageous structure. Metal aerogels consist of randomly ordered and aggregated metal nanoparticles that form self-supporting, highly porous 3D networks, combining the properties of metals (excellent electric conductivity and high catalytic activity/selectivity) and aerogels (low density, broad pore size distribution, and large surface area) in one material [11,12]. Despite their excellent catalytic properties, the scalable production of metal aerogels, in particular, is a critical issue when it comes to their large-scale application. To achieve a simple synthesis design, which extends the range of metal aerogels and creates new gel morphologies, different synthesis approaches have been investigated, such as the one- and two-step syntheses [1,13], freeze-assisted gelation [14,15], a combustion approach [16], or different scalable approaches [17–19]. Furthermore, synthesis parameters, such as reducing agents [20], ligands [21], temperature [22], or even the destabilization method [6,23], have been investigated deeply to further understand and optimize the synthesis of metal aerogels.

One parameter that has rarely been investigated so far is the solvent used in the synthesis. They not only serve as reaction media in the metal gel synthesis, but can act as initiators for the gelation itself as well. Adding a different solvent to a colloidal nanoparticle (NP) solution can alter both, the polarity and the surface potential of the nanoparticles, e.g., attenuating their stabilization, enhancing the attractive interactions between the particles, and thus triggering gelation [12,24].

By default, the synthesis of metal aerogels is carried out in water. H₂O is an environmentally friendly, inexpensive solvent and is available in large quantities. Additionally, the synthesis of metal nanoparticles, which often serve as the building blocks for metal gels, is well established in water [25–31]. Sporadic examples have shown that the metal aerogel synthesis is also possible in other solvents. Abad et al. synthesized gels from Pd nanosheets in various carboxylic acids [32], while Naskar et al. destabilized Pt nanocubes in hexane using hydrazine to successfully initiate gelation [33]. Coaty et al. used hexane as solvent to develop a scalable metal gel synthesis of different transition metals through the reduction of metal halides with organolithium reductants [19]. Another scalable, versatile high-concentration approach in EtOH has shown that the choice of solvent has the potential to shorten the gelation time and reduce the formation of oxides in less noble metal gels. This entails many benefits in terms of large-scale production and enables a wider variety of metal aerogels. In addition, this study provided insights into the effect of low temperature on the gelation process, which would not be possible in H₂O [34]. Based on this approach, bimetallic IrPd gels were synthesized and applied as peroxidase mimics [35].

However, the direct influence and comparison of different solvents regarding the resulting gel morphologies and properties has never been examined. Therefore, this work aims to demonstrate and investigate the influence of the solvent on the gelation itself and the resulting gel networks using Au-Cu as a model system. This metal combination has already received considerable attention in the literature as an electrocatalyst and consists of both a noble and a less-noble metal part [36–39]. Water serves as the standard solvent for the synthesis of the Au_xCu_y gels in this study. Ethanol was selected as the second solvent, because many precursors are readily soluble in ethanol, it is easy to handle, universally applicable, and it has been used sparingly in the metal gel synthesis, although it has shown promising benefits as mentioned above [34]. In addition, ethanol is less toxic than other organic solvents, making its use more likely in future large-scale applications. The prepared samples were studied concerning their morphology via scanning electron microscopy (SEM) and transmission electron microscopy (TEM), their crystal structure via powder X-ray diffraction (XRD), their element distribution with the help of scanning transmission electron microscopy coupled with energy-dispersive X-ray spectroscopy (STEM-EDX), and their porosity via N₂ physisorption in order to link the influence of the solvent with their formation and properties.

2. Results and Discussion

Briefly, Au_xCu_y aerogels were synthesized in three different ratios (Au₃Cu, AuCu, and AuCu₃) via co-reduction, based on the one-step gelation from Liu et al. [1]. Under ambient conditions, the metal salts were reduced in two solvents, water and ethanol, with NaBH₄ serving as the reductant. To maximize comparability, identical concentrations of the metal salts and metal ratios as well as degassing times of the solutions were applied for both approaches. Only the stirring time and the amount of reducing agent differs between them, which can be attributed to optimization experiments previously performed to obtain gel strands that are as homogeneous and thin as possible. The detailed experimental procedure is stated in Section 3.2.

In the aqueous approach, the color of the metal salt solution changes from light yellow to dark brownish-red and turns black after a few hours, while in the ethanolic approach, the solution turns black immediately upon NaBH₄ injection (see Figure S1). This observation indicates the formation of Au_xCu_y NPs and their subsequent aggregation [40]. The abrupt coloration is a sign of the metal reduction [41,42], and a darkening of the solution suggests the growth or aggregation of the reduced species. The absence of the intermediate red-brownish color of the colloids in EtOH indicates faster reaction kinetics and the formation of larger structures compared to the aqueous approach. This matches with the faster formation of black, voluminous precipitates at the bottom of the reaction flask in EtOH (1 day), compared to H₂O (2 days).

TEM analysis of the Au_xCu_y compositions proves the successful formation of homogeneous, highly interconnected gel networks (see Figure 1a,b) for both solvents. Moreover, the overall composition of the precipitates corresponds to the molar ratio of the metal precursors (see Table S1). It can be assumed that the gelation mechanism for the Au–Cu system in water and ethanol is similar to that described by our group in previous reports [1,20,43,44]: Reduction of the metal salt precursors leads to the formation of transiently stabilized NP solutions, followed by a spontaneous gelation due to the decomposition of BH_4^- to the weaker ligand BO_2^- . However, the use of different solvents also leads to significant differences. The faster reaction kinetics for the gelation in EtOH can be attributed to its lower dielectric constant/permittivity (16.2) compared to water (80.3) [45,46], leading to the formation of smaller solvent shells around the transiently stabilized nanoparticles. As a result, faster diffusion of nanoparticles takes place and their ability to come into closer contact without encountering repulsive forces increases. As a result, their aggregation time is significantly reduced [34].

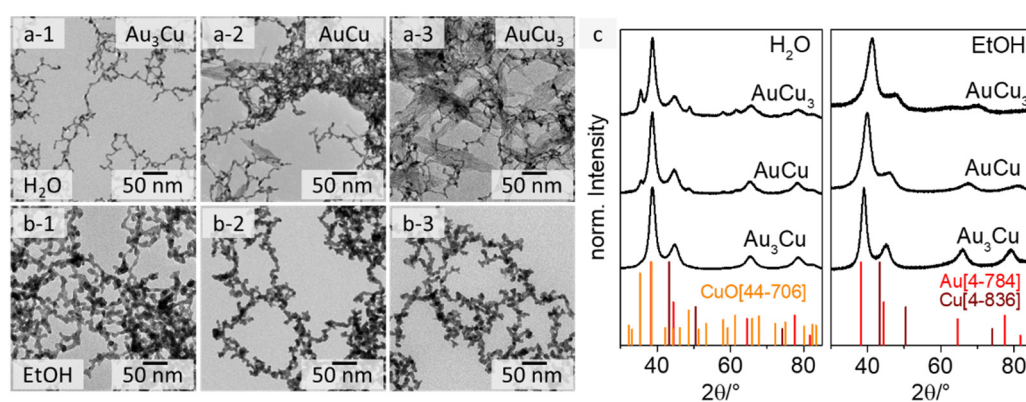


Figure 1. TEM images of Au_3Cu (1), $AuCu$ (2), and $AuCu_3$ (3) aerogels from an aqueous synthesis (a) with an occurring needle-shape side phase for the Cu-rich compositions and from an ethanolic synthesis (b) without side phase. XRD analysis (c) shows the crystalline structure of the Au_xCu_y gels and additional Bragg reflections of CuO for the gels from the aqueous approach.

Regarding the morphology of the gel structures, the web thicknesses (diameter of the gel strands) of the gels from the aqueous approach (see Figure 1a) are (3.2 ± 0.8) nm for Au_3Cu , (2.8 ± 0.6) nm for $AuCu$ and (2.5 ± 0.7) nm for $AuCu_3$, while those for the ethanolic approach are approximately twice as large ((6.7 ± 1.3) nm for Au_3Cu , (6.4 ± 1.1) nm for $AuCu$, and (6.8 ± 1.1) nm for $AuCu_3$) (see Figures 1b and S2). In addition, the gel strands from the aqueous approach are smooth and the NPs are fused together, while the gels derived from the ethanolic synthesis show necklace-like gel strands where the NPs are fused more loosely. The extent of this seems to correlate with the Cu content (see Figures 1 and S6—HAADF-STEM images). In terms of the permittivity, the reaction rate and even the stability of $NaBH_4$ changes in ethanol. The reduction rate of sodium borohydride is faster in EtOH than in H_2O , but its hydrolysis and decomposition are suppressed [47,48]. Consequently, the stabilization of the transiently formed nanoparticles in EtOH is insufficient, which is why the gels' web thicknesses and size distributions differ from those of the aqueous approach [49]. It is also possible that the gelation mechanism shifts towards diffusion-limited cluster aggregation, because the energy required to overcome the coulomb barrier for particle aggregation is lower due to the smaller solvent shell [50]. However, further studies are needed to confirm these assumptions. The reason for the increased particulate gel strands could be the partial oxidation and thus passivation of the gels.

The main difference between the aqueous and ethanolic gels is evident when comparing the TEM and SEM images for the copper-rich compositions $AuCu$ and $AuCu_3$ (see Figures 1(a-2,a-3,b-2,b-3) and S3). Three-dimensional porous network structures were obtained in both solvents. However, the formation of a needle-shaped sub-structure is observed only for the gels synthesized in water with a Cu content ≥ 50 at%. This structure

covers the entire gel network, while no additional phase occurs in EtOH. Analogous observations have previously been made for PtCu aerogels, where the needle-like structure could be identified as CuO [51]. We made similar observations for the Au-Cu system, following XRD analysis (see Figure 1c). XRD measurements for all Au_xCu_y compositions reveal their crystalline face-centered cubic structure, independent from the chosen solvent. Depending on their composition (and following Vegard's rule) [52] the Bragg reflections of the gels shift from the monometallic Au to the monometallic Cu reference. The incorporation of Cu into the Au crystal lattice leads to a shrinkage of the lattice parameters, due to the smaller size of the copper atoms. This results in a shift of the diffraction peak in the XRD pattern, depending on the Au:Cu ratio in the structure. The shift of the Bragg peaks is even more pronounced for the gels from the ethanolic synthesis than for those from the aqueous synthesis. This indicates that significantly more copper is incorporated into the Au-Cu alloy prepared in EtOH. For the aqueous approach, the peak shift for AuCu and AuCu₃ is less pronounced, because some of the copper is used to form an additional copper(II) oxide phase. The relative intensity of the CuO diffraction maxima is increased for AuCu₃ compared to AuCu, which is due to the formation of a larger oxide phase. This is consistent with the observations from the electron microscopy images. Thus, the XRD measurements clearly confirm that the synthesis in ethanol can successfully suppress the oxidation of copper during the formation and gelation of Au_xCu_y nanoparticles under ambient conditions. That can be mainly explained by the faster kinetics of the partial reaction steps and the less oxidative reaction environment (EtOH) during gelation compared to H₂O.

To further demonstrate the advantage of EtOH as a solvent, we prepared a monometallic Cu gel and other bimetallic gold gels (Au₃Ni, Au₃Co, and Au₃Fe) in both solvents, similar to the Au_xCu_y gels (see Figures S4 and S5). In contrast to the reduction of copper chloride in water, which leads exclusively to the formation of needle-shaped CuO (see Figure S4a), a three-dimensional, porous gel network can be obtained in ethanol (see Figure S4b,c) under identical reaction conditions. Again, for the aqueous approach, XRD analysis (Figure S4d) confirms, that only CuO is formed, while metallic Cu and CuO can be detected in EtOH. Most likely, a passivating oxide layer forms around the metallic copper when it gets in contact with air. A similar trend can be observed for the bimetallic Au₃X (X = Ni, Fe, Co) gels (see Figure S5). In water (Figure S5a), some of the samples show non-aggregated single nanoparticles (for Au₃Ni) or large side structures (for Au₃Fe), while in ethanol (Figure S5b), more uniform gel networks are formed that cannot be distinguished morphologically.

For bimetallic systems, the element distribution is key to their potential applications, especially in catalysis. For this reason, the element distributions of the Au_xCu_y gels were investigated using spectrum imaging based on EDX analysis in scanning TEM mode (see Figures 2 and S6). The gels from both synthesis routes (aqueous and ethanolic) show similar element distributions, regardless of their initial Au:Cu ratio. Gold (blue) and copper (red) are quite homogeneously distributed over the whole gel network. However, the homogeneity seems to be slightly better for the ethanolic approach than for the aqueous approach. This may be the result of the faster reaction kinetics of the metal salts in ethanol and the suppressed formation of the CuO phase. Both synthesis routes also show a slight accumulation of oxygen (yellow) on the gel strand surface, indicating oxidation of the nanostructured metals by contact with air, leading to passivation of the aerogels.

The presence of CuO in the AuCu and AuCu₃ hydrogels (aqueous approach) prevents their use in future applications. On the one hand, the influence of the gel network and the oxide needles on their properties can neither be precisely assigned nor distinguished. On the other hand, the oxidation of Cu itself is a process that cannot be prevented and the oxidation does not allow to adjust specific Au:Cu ratios. To remove the copper oxide needles from the gel, an acid post-treatment step can be applied. In particular, carboxylic acids are known to gently dissolve CuO [53,54]. Furthermore, formic acid (HCOOH) has proven to be a selective etchant for CuO in the presence of metallic copper [55–57]. Consequently, the AuCu and AuCu₃ gels were treated with diluted formic acid solutions for 24 h and then purified with water (see Section 3.3) before solvent exchange to acetone

and subsequent supercritical drying. The least concentration of HCOOH to remove all CuO was found to be 14.6 mM (AuCu) and 21.8 mM (AuCu₃) per batch of gel in 20 mL solution in preliminary experiments. This corresponds to a five- and seven-fold excess of acid in relation to the theoretically available amount of Cu in each gel. The usage of larger amounts of acid (24-fold excess of acid) leads to a macroscopic shrinkage of the gel network, which results in the collapse of its structure and an increase of the web thickness (4.9 ± 1.3 nm for AuCu₃) (Figure S7). We assume that, due to the high ionic strength of the solution after adding a large excess of acid, the gel strands aggregate with each other.

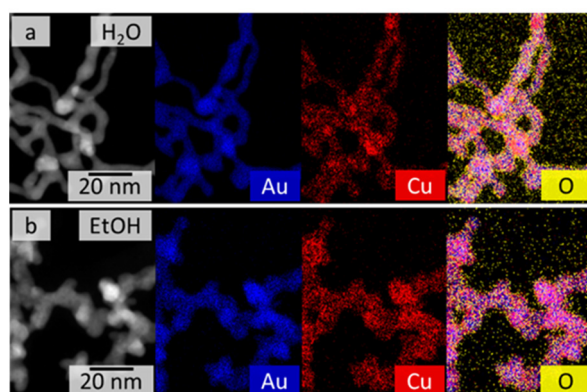


Figure 2. HAADF-STEM images (left) and EDX-based element distributions of the AuCu gel synthesized in water (a) and ethanol (b). Both gels demonstrate a quite homogeneous distribution of Au and Cu over the entire gel networks.

The gel networks of both ratios AuCu and AuCu₃ were almost completely covered with the oxide needles before the acid washing (AW) (see Figure 3(a-1,b-1)). Only after the post-treatment, the typical metal gel network appears and no CuO needles can be found via electron microscopy, which indicates the successful removal of the CuO (see Figure 3(a-2,b-2)) even when the samples were exposed to air again. This assumption can be confirmed by the corresponding XRD analysis (see Figure 3c). The copper oxide diffraction peaks do not appear anymore after the acid treatment, but the crystalline structure of the Au_xCu_y alloys remains intact. Only a small shoulder at the shifted gold diffraction peak is observable for the AuCu₃ sample that fits to the peak with the highest intensity of the CuO pattern. However, since its intensity is very low and no other peaks are found that indicate the formation of an oxide phase, it can be assumed that oxidation of copper reoccurs only to a small extent due to the storage and characterization of the gel at air. Since, as already mentioned above, no needle-like structure can be found, it can be concluded that only surface-near copper is oxidized. It should be possible to remove this kind of oxide layer in future electrocatalytic applications by performing facile cleaning CVs. In-depth studies of the formation of this oxide could be made using X-ray photoelectron spectroscopy (XPS), but this is outside the objective of this article.

Both the TEM and the STEM-EDX results (see Figure S8) show that the gel strands are not affected by the acid. Moreover, both Au and Cu are quite homogeneously distributed in the gel network, demonstrating the successful selective etching of CuO.

Although acid washing selectively removed the undesired CuO side phase and homogeneous, thin Au_xCu_y gels (≈ 3 nm web thickness, see Figure S2) were obtained, the determination of the composition of the aerogels after the HCOOH treatment (see Table S1) shows that both gels have similar compositions of Au₆₂Cu₃₈. Due to the non-controllable oxidation of the copper, it is not possible to adjust the element composition in the gels by this post-treatment method.

The different widths of the Au_xCu_y metal gel strands obtained from the synthesis in H₂O and EtOH have a particular effect on the porosity of the resulting gel networks. Hence, the porosity, respectively a large surface area, is essential for a catalyst application, N₂ physisorption measurements were performed on all Au_xCu_y gels discussed so far. Each

of them, regardless of composition or synthesis route, shows a mixture of type II and IV isotherms, indicating the presence of a broad pore size distribution and the presence of micro-, meso-, and macropores (see Figures 4a and S9) [1]. The corresponding specific surface areas (SSA) and total pore volumes (TpV) are displayed in Table S1. The TpVs range from $0.121 \text{ cm}^3 \text{ g}^{-1}$ to $0.490 \text{ cm}^3 \text{ g}^{-1}$ and thus have typical values for metal aerogels. They increase with elevating copper content for both approaches. The pore volume of both Au_3Cu gels is about $0.120 \text{ cm}^3 \text{ g}^{-1}$, while the pore volumes of the AuCu and AuCu_3 gels from those of the aqueous synthesis ($0.140 \text{ cm}^3 \text{ g}^{-1}$ and $0.213 \text{ cm}^3 \text{ g}^{-1}$) are only half as large as those from the ethanolic one ($0.294 \text{ cm}^3 \text{ g}^{-1}$ and $0.490 \text{ cm}^3 \text{ g}^{-1}$). However, to explain these differences solely by the different solvents chosen is only indirectly correct in this case. On the one hand, the formation of the copper oxide needles ensures a reduction of the pore volume (see acidic washed gels, whose TpVs are higher), and on the other hand, the mass-related volume also must be taken into account, which makes comparability difficult due to the different final element compositions of the aerogels.

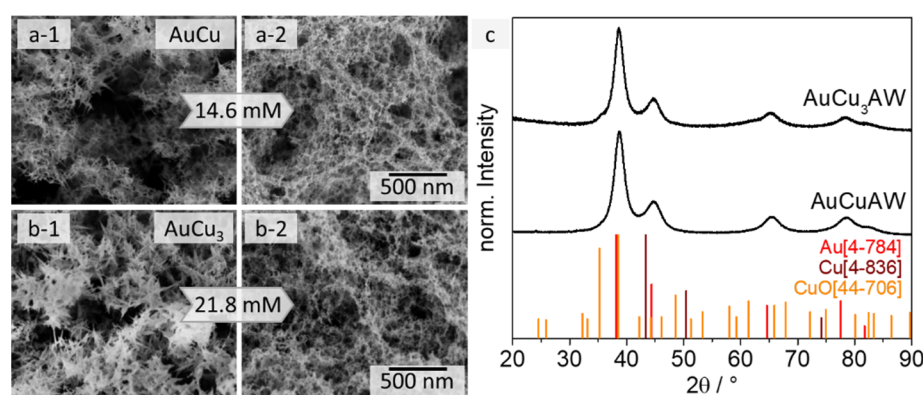


Figure 3. SEM images of AuCu (a) and AuCu_3 (b) gels before (1) and after (2) the acid treatment with HCOOH. The gel networks are covered with CuO needles before the acid washing, which disappear after the HCOOH treatment and the sponge-like gel structure remains. XRD measurements (c) prove the successful removal of the CuO side phase.

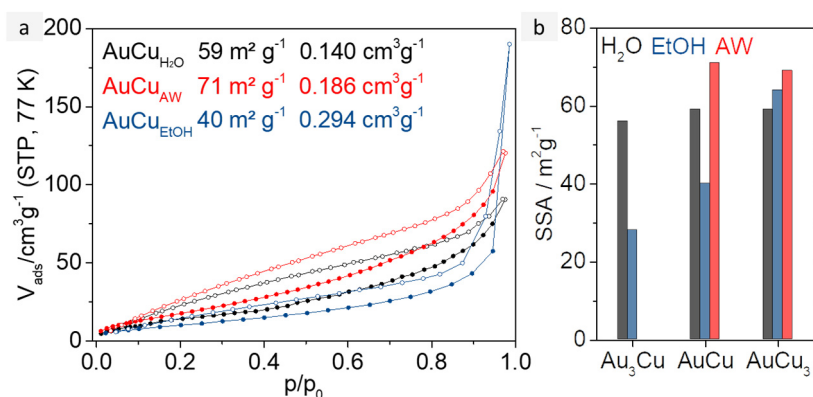


Figure 4. (a) N_2 physisorption isotherms of Au_xCu_y aerogels synthesized in water (black), after acid treatment with HCOOH (red), and synthesized in EtOH (blue). All samples show typical mixtures of type II and IV isotherm, indicating a broad pore size distribution. (b) Specific surface areas for all Au_xCu_y aerogels depending on their compositions and the solvent they were synthesized in.

A graphical overview of the SSAs can be found in Figure 4b. Au_xCu_y aerogels from the aqueous synthesis have large SSAs of 56 to $59 \text{ m}^2 \text{ g}^{-1}$. However, it should be noted that CuO generates additional surface and interparticular cavities, but can also block pores and thus reduce the SSA. After acid washing, the specific surface area increases slightly to about $70 \text{ m}^2 \text{ g}^{-1}$ for AuCu and AuCu_3 . On the one hand, surface area is lost by removing

the CuO, on the other hand, blocked pores are exposed and oxide layers on the gel surface are also removed. This leads to slightly thinner strands and therefore to larger SSAs. In comparison, the SSAs of the aerogels from the ethanolic synthesis are in a range of 28 to 64 m²g⁻¹, depending on their composition. This drastic difference is mainly caused by the doubled web thickness of the aerogels, compared to the ones from the aqueous synthesis. Furthermore, the necklace-like structure of the ethanolic gels with higher Cu content acts beneficially for their surface area. This effect could explain why the SSA of the ethanolic AuCu₃ gel is larger than its aqueous counterpart.

3. Materials and Methods

3.1. Chemicals

The following chemicals were used as purchased: hydrogen tetrachloroaurate(III) trihydrate (HAuCl₄·3 H₂O; 99.99%; abcr GmbH; Germany), copper(II) chloride (CuCl₂; 99.995%; Fischer Scientific (Thermo Fisher Scientific, Kandel, Germany), nickel(II) chloride (NiCl₂; 99.995%; Alfa Aesar (Thermo Fisher Scientific, Kandel, Germany), cobalt(II) chloride (CoCl₂; 99.9%; Alfa Aesar (Thermo Fisher Scientific, Kandel, Germany), iron(II) chloride tetrahydrate (FeCl₂·4 H₂O; 99%; Gruessing GmbH, Filsum, Germany), sodium borohydride (NaBH₄; 99.99%; Sigma Aldrich, Darmstadt, Germany), formic acid (HCOOH; 98–100%; Riedel de Haën, Seelze, Germany), denatured ethanol (EtOH; 99 + 1% petroleum ether; Berkel AHK, Ludwigshafen, Germany), acetone (99.9%; Acros Organics (Thermo Fisher Scientific, Kandel, Germany), Milli-Q water (18.2 MΩ). Stock solutions (50 mM) of NaBH₄ and each metal salt were prepared in H₂O and EtOH.

3.2. Synthesis of Au-Cu Aerogels

The synthesis of Au_xCu_y aerogels is based on the following procedure: A total amount of 0.1 mmol metal salt precursor (molar ratio of the precursors defines the product ratio Au:Cu) was diluted in 400 mL solvent (H₂O or EtOH). The solution was degassed for 30 min under stirring (450 rpm) with nitrogen to impede oxidation. Subsequently, a defined volume of a 50 mM NaBH₄ solution (water or ethanol) was rapidly added and the reaction mixture was further stirred (120 s for H₂O; 30 s for EtOH) under bubbling with N₂. The ratio of reduction equivalents to metal ion equivalents ($n_{H^-} : n_{Me^+}$) was determined to be 12 for the aqueous and 6 for the ethanolic synthesis. After the N₂ bubbling was stopped, the reaction mixture was stored for 1–2 days until the intermediate formed nanoparticles were completely gelled and settled down. The obtained gels were collected and washed 7 times within 3 days with the respective solvent to remove the remaining residuals. Afterwards, for the aqueous synthesis, the water was stepwise exchanged to acetone. Finally, the solvogels (in acetone or EtOH) were transferred into an autoclave, the solvents exchanged to CO₂, and a supercritical drying process was performed at 37 °C and 90 bar to obtain the aerogels. The samples were stored in air before further characterization. The syntheses of Au₃Ni, Au₃Co, Au₃Fe, and pure Cu aerogels were performed similarly to the Au_xCu_y gels. Only the respective metal precursors were exchanged.

3.3. Acid Post-Treatment

For the acid post-treatment, the washed AuCu and AuCu₃ hydrogels were transferred to 20 mL of an aqueous solution containing 11.1 μL and 16.6 μL formic acid respectively. After gently shaking, the solvogels were left in the acidic solution for 24 h under ambient conditions. The dissolved species were finally removed by consecutively washing the gels with water three times. Further processing (e.g., solvent exchange) was performed in accordance with the above-mentioned procedure. All other gels (Au₃Cu or Au₃X) were not treated with formic acid.

3.4. Instruments and Characterization

The supercritical drying was performed in an autoclave type 13200J0AB from Spi Supplies. The structural and compositional analysis was realized via electron microscopy. For

this, a transmission electron microscope (TEM) JEOL/EO JEM-1400plus (120 kV), equipped with a LaB₆ cathode, was used for bright-field imaging. To determine the average web thickness of the aerogels, the widths of the gel strands were determined at approximately 200 different spots. For high-angle annular dark-field (HAADF) imaging in scanning TEM (STEM) mode as well as element mapping based on energy-dispersive X-ray spectroscopy (EDX), a Talos F200X microscope (200 kV) equipped with an X-FEG emission gun and a Super-X EDX detector from FEI (Thermo Fisher Scientific, Waltham, MA, USA) was used. The three-dimensional porous structures of the aerogels and their element composition were investigated via scanning electron microscopy (SEM) and energy-dispersive X-ray spectroscopy (EDX) with an FESEM SU8020 from Hitachi (2 kV, 10 μA) combined with a Silicon Drift Detector 80 X-Max^N from Oxford Instruments (20 kV, 10 μA). X-ray diffraction (XRD) was carried out with a Bruker Phaser D2 (Cu Kα = 1.5406 Å, Bruker Corp., Billerica, MA, USA) to study the crystallinity of the aerogels. The International Centre for Diffraction Data (ICDD) database was used to generate the peak positions of the XRD reference patterns. A Nova3000e from Quantachrome was used to determine the nitrogen adsorption capability, the resulting specific surface area (SSA) and the total pore volume (TpV) at $p/p_0 = 0.98$, standard temperatures (77 K), and standard pressure (1 atm) (STP).

4. Conclusions

In this work, we demonstrated the ligand-free synthesis of Au_xCu_y aerogels under ambient conditions in water and ethanol. We showed that the choice of the solvent has a noticeable impact on the morphology, gelation time, and porosity of the gels. However, the crystallinity and element distributions do not seem to be affected by changing this parameter. While the synthesis in water leads to the formation of smooth gel strands with web thicknesses of about 3 nm and networks with SSAs of 56 to 59 m²g⁻¹, in ethanol particulate gel strands with a doubled web thickness and gels with specific surface areas of 28 to 64 m²g⁻¹ are formed. In addition, we observed the formation of a CuO side phase in the AuCu and AuCu₃ gels from the aqueous synthesis, while the synthesis in ethanol suppresses the copper oxidation. Furthermore, we found that the synthesis in ethanol almost halves the gelation time. These advantages allowed us to synthesize Au_xCu_y aerogels in well-defined compositions as well as pure Cu gels.

On the one hand, we can attribute the different results in gelation to the low permittivity of EtOH, as this leads, among other phenomena, to smaller solvent shells, which reduces the repulsion of the transiently formed nanoparticles and leads to higher reaction and gelation rates. On the other hand, the reaction and hydrolysis rates of the reducing agent in EtOH are also changed, which has a lasting effect on the stabilization of the transiently formed nanoparticles. As a side experiment, we were able to selectively remove the formed oxide phase for the AuCu and AuCu₃ gels from the aqueous synthesis using formic acid as etchant in a post-synthetic washing step. Moreover, for further bimetallic Au₃X systems (X = Fe, Ni, Co), we were able to show the advantage of their gelation in ethanol compared to their synthesis in water.

In summary, we demonstrated the importance and potential of the choice of solvent in the preparation of metal aerogels, especially in terms of optimizing the synthesis time or the preparation of less-noble metal aerogels. We could show that only by changing the solvent, at otherwise constant parameters, the gelation time of metal aerogels can be halved and oxidation of less noble metals can be suppressed. These improvements could previously only be achieved by elevated gelation temperatures [22], stirring during gelation [58], the use of highly concentrated solutions [17–19,34], or the addition of ligands/hard to remove additives [19]. Our approach takes place at room temperature, only using the solvent, the metal precursors, and the reducing agent as reactant, with no other external influences, except short stirring to mix the reactants. However, the approach is limited mainly by the poor solubility of the precursors in EtOH and the higher toxicity/lower availability of ethanol and other possible organic solvents compared to water. It should be possible to reverse the biggest drawback of the ethanolic approach (increased web thickness) by

using lower metal precursor concentrations. In the future, other solvents or even the use of solvent mixtures should be investigated to further understand the influence of the permittivity on the gelation of metal aerogels and to circumvent limitations of this approach. Ultimately, the performance of aerogels in electrocatalysis is crucial for their application. This is the aspect to which our ongoing research is devoted for some of the materials presented in this article, in order to complete the picture regarding the influence of the solvents for applicability to metal aerogels.

Supplementary Materials: The following supporting information can be downloaded at: <https://www.mdpi.com/article/10.3390/catal12040441/s1>, Table S1: Properties of all Au_xCu_y aerogels prepared via a synthesis in H_2O and EtOH. Element compositions were determined via SEM-EDX and SSA/TpV via N_2 physisorption; Figure S1: Time lapse photographs of the Au_3Cu solvogel gelation process in water (left) and ethanol (right). The metal salt solutions turn dark upon $NaBH_4$ addition. The intermediately formed aggregates settle at different rates and form gels; Figure S2: Overview of the web thicknesses and their distribution of all prepared $AuxCuy$ aerogels, determined from the bright-field TEM images and visualized in the form of boxplots. The average web thickness of the gels prepared in aqueous solution is 3 nm, while that of the gels prepared in ethanolic solution is about 6 nm. In EtOH, the web thickness distribution becomes broader; Figure S3: SEM images of Au_3Cu (1), AuC_u (2), and AuC_u_3 (3) aerogels from an aqueous (a) and ethanolic (b) synthesis. The aerogels form three-dimensional, porous networks. In a-2 and a-3 the gels are covered with a needle-like substructure; Figure S4: TEM (a + b) and SEM (c) images as well as XRD analysis (d) of reduced $CuCl_2$, following the synthesis parameter of the Au-Cu gels. In water (a) the reaction leads to the formation of CuO-needles (d). In EtOH the formation of a three-dimensional Cu aerogel (b + c) can be observed. The gel keeps its metallic character and an additional CuO phase (d); Figure S5: TEM images of Au_3Ni (1), Au_3Fe (2) and Au_3Co (3) gels, synthesized in H_2O (a) and EtOH (b). The synthesis results in irregular gel structures in water, while similar gel morphologies are obtained in ethanol; Figure S6: HAADF-STEM images (left) and EDX-based element distributions of the Au_3Cu (1) and AuC_u_3 (2) gels synthesized in water (a) and ethanol (b). The gels demonstrate a quite homogeneous distribution of Au and Cu over the whole gel networks; Figure S7: AuC_u_3 gel before (a) and after (b) the acid treatment in a 88.5 mM formic acid solution. TEM image (c) of the acid-treated gel. The treatment leads to a macroscopic shrinkage of the structure and an increase of the web thickness; Figure S8: TEM micrographs as well as HAADF-STEM images and EDX-based element distributions of the AuC_u (a) and AuC_u_3 (b) gels from the aqueous approach after the acid treatment with HCOOH. CuO is not observable and the gel network remains untouched. Cu can still be found in the gel strands; Figure S9: N_2 physisorption isotherms of Au_3Cu (a) and AuC_u_3 (b) aerogels synthesized in water (black), after acid treatment with HCOOH (red) and synthesized in EtOH (blue). All isotherms are combinations of type II and IV, indicating broad pore size distributions.

Author Contributions: Conceptualization, M.G., J.K. and A.E.; methodology, all authors; validation, M.G., J.K., K.H. and R.H.; formal analysis, M.G., J.K., K.H. and R.H.; investigation, M.G., J.K., K.H. and R.H.; resources, R.H. and A.E.; data curation, M.G., J.K., R.H. and A.E.; writing—original draft preparation, M.G.; writing—review and editing, all authors; visualization, M.G. and J.K.; supervision, A.E.; project administration, M.G. and A.E.; funding acquisition, K.H., R.H. and A.E. All authors have read and agreed to the published version of the manuscript.

Funding: This research was funded by the German Federal Ministry of Education and Research (BMBF), grant number 03SF0451, the German Research Foundation (DFG), grant number EY 16/18-2 and the European Research Council (ERC), AdG AEROCAT, grant number 3404109 and PoC LAACat, grant number 875564.

Data Availability Statement: The data presented in this study are available on request from the corresponding author.

Acknowledgments: The authors would like to thank Nelli Weiß and Benjamin Klemmed for recording the bright-field TEM images. The use of the HZDR Ion Beam Center TEM facilities is acknowledged.

Conflicts of Interest: The authors declare no conflict of interest.

References

1. Liu, W.; Rodriguez, P.; Borchardt, L.; Foelske, A.; Yuan, J.; Herrmann, A.K.; Geiger, D.; Zheng, Z.; Kaskel, S.; Gaponik, N.; et al. Bimetallic Aerogels: High-Performance Electrocatalysts for the Oxygen Reduction Reaction. *Angew. Chem. Int. Ed.* **2013**, *52*, 9849–9852. [[CrossRef](#)] [[PubMed](#)]
2. Henning, S.; Ishikawa, H.; Kühn, L.; Herranz, J.; Müller, E.; Eychmüller, A.; Schmidt, T.J. Unsupported Pt-Ni Aerogels with Enhanced High Current Performance and Durability in Fuel Cell Cathodes. *Angew. Chem. Int. Ed.* **2017**, *56*, 10707–10710. [[CrossRef](#)] [[PubMed](#)]
3. Du, R.; Jin, W.; Wu, H.; Hübner, R.; Zhou, L.; Xue, G.; Hu, Y.; Eychmüller, A. Rapid Synthesis of Gold-Palladium Core-Shell Aerogels for Selective and Robust Electrochemical CO₂ reduction. *J. Mater. Chem. A* **2021**, *9*, 17189–17197. [[CrossRef](#)]
4. Lu, L.; Sun, X.; Ma, J.; Yang, D.; Wu, H.; Zhang, B.; Zhang, J.; Han, B. Highly Efficient Electroreduction of CO₂ to Methanol on Palladium-Copper Bimetallic Aerogels. *Angew. Chem. Int. Ed.* **2018**, *57*, 14149–14153. [[CrossRef](#)]
5. Jiang, X.; Du, R.; Hübner, R.; Hu, Y.; Eychmüller, A. A Roadmap for 3D Metal Aerogels: Materials Design and Application Attempts. *Matter* **2021**, *4*, 54–94. [[CrossRef](#)]
6. Ziegler, C.; Wolf, A.; Liu, W.; Herrmann, A.K.; Gaponik, N.; Eychmüller, A. Modern Inorganic Aerogels. *Angew. Chem. Int. Ed.* **2017**, *56*, 13200–13221. [[CrossRef](#)]
7. Zheng, Y.; Yang, J.; Lu, X.; Wang, H.; Dubale, A.A.; Li, Y.; Jin, Z.; Lou, D.; Sethi, N.K.; Ye, Y.; et al. Boosting Both Electrocatalytic Activity and Durability of Metal Aerogels via Intrinsic Hierarchical Porosity and Continuous Conductive Network Backbone Preservation. *Adv. Energy Mater.* **2021**, *11*, 2002276. [[CrossRef](#)]
8. Wang, H.; Fang, Q.; Gu, W.; Du, D.; Lin, Y.; Zhu, C. Noble Metal Aerogels. *ACS Appl. Mater. Interfaces* **2020**, *12*, 52234–52250. [[CrossRef](#)]
9. Wang, H.; Jiao, L.; Zheng, L.; Fang, Q.; Qin, Y.; Luo, X.; Wei, X.; Hu, L.; Gu, W.; Wen, J.; et al. PdBi Single-Atom Alloy Aerogels for Efficient Ethanol Oxidation. *Adv. Funct. Mater.* **2021**, *31*, 2103465. [[CrossRef](#)]
10. Gao, W.; Lei, M.; Li, L.; Wen, D. Promoting the Electrocatalytic Properties of Nickel Aerogel by Gold Decoration for Efficient Electrocatalytic Oxygen Evolution in Alkali. *Chem. Commun.* **2020**, *56*, 15446–15449. [[CrossRef](#)]
11. Bigall, N.C.; Eychmüller, A. Synthesis of Noble Metal Nanoparticles and Their Non-Ordered Superstructures. *Philos. Trans. R. Soc. A Math. Phys. Eng. Sci.* **2010**, *368*, 1385–1404. [[CrossRef](#)] [[PubMed](#)]
12. Bigall, N.C.; Herrmann, A.K.; Vogel, M.; Rose, M.; Simon, P.; Carrillo-Cabrera, W.; Dorfs, D.; Kaskel, S.; Gaponik, N.; Eychmüller, A. Hydrogels and Aerogels from Noble Metal Nanoparticles. *Angew. Chem. Int. Ed.* **2009**, *48*, 9731–9734. [[CrossRef](#)] [[PubMed](#)]
13. Herrmann, A.K.; Formanek, P.; Borchardt, L.; Klose, M.; Giebler, L.; Eckert, J.; Kaskel, S.; Gaponik, N.; Eychmüller, A. Multimetallic Aerogels by Template-Free Self-Assembly of Au, Ag, Pt, and Pd Nanoparticles. *Chem. Mater.* **2014**, *26*, 1074–1083. [[CrossRef](#)]
14. Du, R.; Joswig, J.O.; Hübner, R.; Zhou, L.; Wei, W.; Hu, Y.; Eychmüller, A. Freeze-Thaw-Promoted Fabrication of Clean and Hierarchically Structured Noble-Metal Aerogels for Electrocatalysis and Photoelectrocatalysis. *Angew. Chem.* **2020**, *132*, 8370–8377. [[CrossRef](#)]
15. Freytag, A.; Sánchez-Paradinas, S.; Naskar, S.; Wendt, N.; Colombo, M.; Pugliese, G.; Poppe, J.; Demirci, C.; Kretschmer, I.; Bahnemann, D.W.; et al. Versatile Aerogel Fabrication by Freezing and Subsequent Freeze-Drying of Colloidal Nanoparticle Solutions. *Angew. Chem. Int. Ed.* **2016**, *55*, 1200–1203. [[CrossRef](#)] [[PubMed](#)]
16. Leventis, N.; Chandrasekaran, N.; Sadekar, A.G.; Mulik, S.; Sotiriou-Leventis, C. The Effect of Compactness on the Carbothermal Conversion of Interpenetrating Metal Oxide/Resorcinol-Formaldehyde Nanoparticle Networks to Porous Metals and Carbides. *J. Mater. Chem.* **2010**, *20*, 7456–7471. [[CrossRef](#)]
17. Burpo, F.J.; Nagelli, E.A.; Morris, L.A.; McClure, J.P.; Ryu, M.Y.; Palmer, J.L. Direct Solution-Based Reduction Synthesis of Au, Pd, and Pt Aerogels. *J. Mater. Res.* **2017**, *32*, 4153–4165. [[CrossRef](#)]
18. Krishna, K.S.; Sandeep, C.S.S.; Philip, R.; Eswaramoorthy, M. Mixing Does the Magic: A Rapid Synthesis of High Surface Area Noble Metal Nanosponges Showing Broadband Nonlinear Optical Response. *ACS Nano* **2010**, *4*, 2681–2688. [[CrossRef](#)]
19. Coaty, C.; Zhou, H.; Liu, H.; Liu, P. A Scalable Synthesis Pathway to Nanoporous Metal Structures. *ACS Nano* **2018**, *12*, 432–440. [[CrossRef](#)]
20. Du, R.; Wang, J.; Wang, Y.; Hübner, R.; Fan, X.; Senkovska, I.; Hu, Y.; Kaskel, S.; Eychmüller, A. Unveiling Reductant Chemistry in Fabricating Noble Metal Aerogels for Superior Oxygen Evolution and Ethanol Oxidation. *Nat. Commun.* **2020**, *11*, 1590. [[CrossRef](#)]
21. Fan, X.; Zerebecki, S.; Du, R.; Hübner, R.; Marzum, G.; Jiang, G.; Hu, Y.; Barcikowski, S.; Reichenberger, S.; Eychmüller, A. Promoting the Electrocatalytic Performance of Noble Metal Aerogels by Ligand-Directed Modulation. *Angew. Chem.* **2020**, *132*, 5755–5760. [[CrossRef](#)]
22. Shi, Q.; Zhu, C.; Du, D.; Bi, C.; Xia, H.; Feng, S.; Engelhard, M.H.; Lin, Y. Kinetically Controlled Synthesis of AuPt Bi-Metallic Aerogels and Their Enhanced Electrocatalytic Performances. *J. Mater. Chem. A* **2017**, *5*, 19626–19631. [[CrossRef](#)]
23. Du, R.; Hu, Y.; Hübner, R.; Joswig, J.-O.O.; Fan, X.; Schneider, K.; Eychmüller, A.; Hübner, R.; Joswig, J.-O.O.; Fan, X.; et al. Specific Ion Effects Directed Noble Metal Aerogels: Versatile Manipulation for Electrocatalysis and Beyond. *Sci. Adv.* **2019**, *5*, eaaw4590. [[CrossRef](#)] [[PubMed](#)]
24. Hiekel, K.; Jungblut, S.; Georgi, M.; Eychmüller, A. Tailoring the Morphology and Fractal Dimension of 2D Mesh-like Gold Gels. *Angew. Chem. Int. Ed.* **2020**, *59*, 12048–12054. [[CrossRef](#)]

25. Bigall, N.C.; Härtling, T.; Klose, M.; Simon, P.; Eng, L.M.; Eychmüller, A. Monodisperse Platinum Nanospheres with Adjustable Diameters from 10 to 100 Nm: Synthesis and Distinct Optical Properties. *Nano Lett.* **2008**, *8*, 4588–4592. [[CrossRef](#)]
26. Ziegler, C.; Eychmüller, A. Seeded Growth Synthesis of Uniform Gold Nanoparticles with Diameters of 15–300 Nm. *J. Phys. Chem. C* **2011**, *115*, 4502–4506. [[CrossRef](#)]
27. Nemamcha, A.; Rehspringer, J.L.; Khatmi, D. Synthesis of Palladium Nanoparticles by Sonochemical Reduction of Palladium(II) Nitrate in Aqueous Solution. *J. Phys. Chem. B* **2006**, *110*, 383–387. [[CrossRef](#)]
28. Sakai, T.; Ishihara, A.; Alexandridis, P. Block Copolymer-Mediated Synthesis of Silver Nanoparticles from Silver Ions in Aqueous Media. *Colloids Surf. A Physicochem. Eng. Asp.* **2015**, *487*, 84–91. [[CrossRef](#)]
29. Kobayashi, Y.; Shirochi, T.; Yasuda, Y.; Morita, T. Metal-Metal Bonding Process Using Metallic Copper Nanoparticles Prepared in Aqueous Solution. *Int. J. Adhes. Adhes.* **2012**, *33*, 50–55. [[CrossRef](#)]
30. Cai, B.; Wen, D.; Liu, W.; Herrmann, A.K.; Benad, A.; Eychmüller, A. Function-Led Design of Aerogels: Self-Assembly of Alloyed PdNi Hollow Nanospheres for Efficient Electrocatalysis. *Angew. Chem. Int. Ed.* **2015**, *54*, 13101–13105. [[CrossRef](#)]
31. Turkevich, J.; Stevenson, P.C.; Hillier, J. A Study of the Nucleation and Growth Processes in the Synthesis of Colloidal Gold. *Discuss. Faraday Soc.* **1951**, *11*, 55–75. [[CrossRef](#)]
32. Zareie Yazdan-Abad, M.; Noroozifar, M.; Douk, A.S.; Modarresi-Alam, A.R.; Saravani, H. Shape Engineering of Palladium Aerogels Assembled by Nanosheets to Achieve a High Performance Electrocatalyst. *Appl. Catal. B Environ.* **2019**, *250*, 242–249. [[CrossRef](#)]
33. Naskar, S.; Freytag, A.; Deutsch, J.; Wendt, N.; Behrens, P.; Köckritz, A.; Bigall, N.C. Porous Aerogels from Shape-Controlled Metal Nanoparticles Directly from Nonpolar Colloidal Solution. *Chem. Mater.* **2017**, *29*, 9208–9217. [[CrossRef](#)]
34. Georgi, M.; Klemmed, B.; Benad, A.; Eychmüller, A. A Versatile Ethanolic Approach to Metal Aerogels (Pt, Pd, Au, Ag, Cu and Co). *Mater. Chem. Front.* **2019**, *3*, 1586–1592. [[CrossRef](#)]
35. Tan, X.; Yang, Q.; Sun, X.; Sun, P.; Li, H. PdIr Aerogels with Boosted Peroxidase-like Activity for a Sensitive Total Antioxidant Capacity Colorimetric Bioassay. *ACS Appl. Mater. Interfaces* **2022**, *14*, 10047–10054. [[CrossRef](#)]
36. Zhu, C.; Shi, Q.; Fu, S.; Song, J.; Xia, H.; Du, D.; Lin, Y. Efficient Synthesis of MCu (M = Pd, Pt, and Au) Aerogels with Accelerated Gelation Kinetics and Their High Electrocatalytic Activity. *Adv. Mater.* **2016**, *28*, 8779–8783. [[CrossRef](#)]
37. Wang, J.; Chen, F.; Jin, Y.; Johnston, R.L. Gold–Copper Aerogels with Intriguing Surface Electronic Modulation as Highly Active and Stable Electrocatalysts for Oxygen Reduction and Borohydride Oxidation. *ChemSusChem* **2018**, *11*, 1354–1364. [[CrossRef](#)]
38. Zhong, D.; Zhang, L.; Zhao, Q.; Cheng, D.; Deng, W.; Liu, B.; Zhang, G.; Dong, H.; Yuan, X.; Zhao, Z.; et al. Concentrating and Activating Carbon Dioxide over AuCu Aerogel Grain Boundaries. *J. Chem. Phys.* **2020**, *152*, 204703. [[CrossRef](#)]
39. Qin, J.; Tan, X.; Feng, F.; Li, H. Facile and Controllable Synthesis of AuCu Aerogels for the Enhanced Degradation of 4-Nitrophenol. *Appl. Surf. Sci.* **2021**, *561*, 150024. [[CrossRef](#)]
40. Liu, W.; Herrmann, A.K.; Bigall, N.C.; Rodriguez, P.; Wen, D.; Oezaslan, M.; Schmidt, T.J.; Gaponik, N.; Eychmüller, A. Noble Metal Aerogels—Synthesis, Characterization, and Application as Electrocatalysts. *Acc. Chem. Res.* **2015**, *48*, 154–162. [[CrossRef](#)]
41. Van Hying, D.L.; Zukoski, C.F. Formation Mechanisms and Aggregation Behavior of Borohydride Reduced Silver Particles. *Langmuir* **1998**, *14*, 7034–7046. [[CrossRef](#)]
42. Song, Y.; Garcia, R.M.; Dorin, R.M.; Wang, H.; Qiu, Y.; Coker, E.N.; Steen, W.A.; Miller, J.E.; Shelnut, J.A. Synthesis of Platinum Nanowire Networks Using a Soft Template. *Nano Lett.* **2007**, *7*, 3650–3655. [[CrossRef](#)] [[PubMed](#)]
43. Henning, S.; Kühn, L.; Herranz, J.; Durst, J.; Binninger, T.; Nachtegaal, M.; Werheid, M.; Liu, W.; Adam, M.; Kaskel, S.; et al. Pt-Ni Aerogels as Unsupported Electrocatalysts for the Oxygen Reduction Reaction. *J. Electrochem. Soc.* **2016**, *163*, F998–F1003. [[CrossRef](#)]
44. Deraedt, C.; Salmon, L.; Gatard, S.; Ciganda, R.; Hernandez, R.; Mayor, M.; Astruc, D. Sodium Borohydride Stabilizes Very Active Gold Nanoparticle Catalysts. *Chem. Commun.* **2014**, *50*, 14194–14196. [[CrossRef](#)] [[PubMed](#)]
45. Mohsen-Nia, M.; Amiri, H.; Jazi, B. Dielectric Constants of Water, Methanol, Ethanol, Butanol and Acetone: Measurement and Computational Study. *J. Solut. Chem.* **2010**, *39*, 701–708. [[CrossRef](#)]
46. Åkerlöf, G. Dielectric Constants of Some Organic Solvent-Water Mixtures at Various Temperatures. *J. Am. Chem. Soc.* **1932**, *54*, 4125–4139. [[CrossRef](#)]
47. Retnamma, R.; Novais, A.Q.; Rangel, C.M. Kinetics of Hydrolysis of Sodium Borohydride for Hydrogen Production in Fuel Cell Applications: A Review. *Int. J. Hydrog. Energy* **2011**, *36*, 9772–9790. [[CrossRef](#)]
48. Brown, H.C.; Ichikawa, K. The Influence of Solvent and Metal Ion on the Rate of Reaction of Alkali Metal Borohydrides with Acetone. *J. Am. Chem. Soc.* **1961**, *83*, 4372–4374. [[CrossRef](#)]
49. Du, R.; Fan, X.; Jin, X.; Hübner, R.; Hu, Y.; Eychmüller, A. Emerging Noble Metal Aerogels: State of the Art and a Look Forward. *Matter* **2019**, *1*, 39–56. [[CrossRef](#)]
50. Weitz, D.A.; Huang, J.S.; Lin, M.Y.; Sung, J. Limits of the Fractal Dimension for Irreversible Kinetic Aggregation of Gold Colloids. *Phys. Rev. Lett.* **1985**, *54*, 1416–1419. [[CrossRef](#)]
51. Henning, S.; Kühn, L.; Herranz, J.; Nachtegaal, M.; Hübner, R.; Werheid, M.; Eychmüller, A.; Schmidt, T.J. Effect of Acid Washing on the Oxygen Reduction Reaction Activity of Pt-Cu Aerogel Catalysts. *Electrochim. Acta* **2017**, *233*, 210–217. [[CrossRef](#)]
52. Vegard, L. Die Konstitution Der Mischkristalle Und Die Raumbfüllung Der Atome. *Zeitschrift für Phys.* **1921**, *5*, 17–26. [[CrossRef](#)]
53. Chavez, K.L.; Hess, D.W. A Novel Method of Etching Copper Oxide Using Acetic Acid. *J. Electrochem. Soc.* **2001**, *148*, G640. [[CrossRef](#)]

54. Qu, G.; Vegunta, S.S.S.; Mai, K.; Weinman, C.J.; Ghosh, T.; Wu, W.; Flake, J.C. Copper Oxide Removal Activity in Nonaqueous Carboxylic Acid Solutions. *J. Electrochem. Soc.* **2013**, *160*, E49–E53. [[CrossRef](#)]
55. Chen, J.K.-C.; Altieri, N.D.; Kim, T.; Lill, T.; Shen, M.; Chang, J.P. Directional Etch of Magnetic and Noble Metals. I. Role of Surface Oxidation States. *J. Vac. Sci. Technol. A Vac. Surf. Film.* **2017**, *35*, 05C304. [[CrossRef](#)]
56. Chen, J.K.-C.; Altieri, N.D.; Kim, T.; Chen, E.; Lill, T.; Shen, M.; Chang, J.P. Directional Etch of Magnetic and Noble Metals. II. Organic Chemical Vapor Etch. *J. Vac. Sci. Technol. A Vac. Surf. Film.* **2017**, *35*, 05C305. [[CrossRef](#)]
57. Altieri, N.D.; Chen, J.K.-C.; Minardi, L.; Chang, J.P. Review Article: Plasma–Surface Interactions at the Atomic Scale for Patterning Metals. *J. Vac. Sci. Technol. A Vac. Surf. Film.* **2017**, *35*, 05C203. [[CrossRef](#)]
58. Du, R.; Joswig, J.-O.; Fan, X.; Hübner, R.; Spittel, D.; Hu, Y.; Eychmüller, A. Disturbance-Promoted Unconventional and Rapid Fabrication of Self-Healable Noble Metal Gels for (Photo-)Electrocatalysis. *Matter* **2020**, *2*, 908–920. [[CrossRef](#)]